SCIENCE CHINA
Information Sciences

• RESEARCH PAPER •

November 2026, Vol. 69, Iss. 11, 210208:1–210208:18
https://doi.org/10.1007/s11432-026-5202-9

Special Topic: Intelligent Characterization and Modeling for Complex Systems

Structural heterogeneity of the Drosophila brain network

Xiaoyu ZHANG[1,2], Pengcheng YANG[1], Yifei ZHANG[1], Bo-Wei QIN[2], Qiang LUO[2], Wei LIN[2*] & Xin LU[1*]

[1]*College of Systems Engineering, National University of Defense Technology, Changsha 410073, China*
[2]*Research Institute of Intelligent Complex Systems, Fudan University, Shanghai 200433, China*

Received 17 March 2026/Revised 15 May 2026/Accepted 18 September 2026/Published online 30 October 2026

Abstract Decoding the heterogeneity of biological neural systems is key to understanding the nervous system's complex dynamical behaviors. This study analyzes the comprehensive Drosophila brain connectome, which is the most recent dataset, containing over 130000 neurons and 50M synapses. We conducted meticulous analyses of both network and spatial structure. Our findings reveal significant heterogeneity in network properties and distinct spatial clustering across functional regions. Besides, our analysis revealed a modular organizational pattern within the neural network, wherein regions with similar functions exhibited higher connection densities, forming distinct community structures. Moreover, we observed spatial clustering within functional regions, but it was not statistically significant. Additionally, we identified pervasive bilateral symmetry in network topology and spatial organization. Simulations based on the Kuramoto model demonstrate that the functional asymmetry between cerebral hemispheres predominantly arises from disparities in the intrinsic frequencies of neurons rather than from structural asymmetry within the neural network itself. These insights advance our understanding of neural network organization and complexity in biological systems.

Keywords connectome, neural heterogeneity, modular organization, bilateral symmetry, Kuramoto model

Citation Zhang X Y, Yang P C, Zhang Y F, et al. Structural heterogeneity of the Drosophila brain network. Sci China Inf Sci, 2026, 69(11): 210208, https://doi.org/10.1007/s11432-026-5202-9

1 Introduction

Neural heterogeneity has emerged as a fundamental concept in modern neuroscience research, profoundly shaping the understanding of the nervous system and therapeutic strategies for neurological disorders [1–3]. From an evolutionary perspective, this heterogeneity represents the product of natural selection, enabling neural systems to cope with complex and dynamic environmental challenges while providing the foundation for species adaptability. At the molecular and cellular levels, neuronal heterogeneity manifests in multiple aspects, including morphological characteristics, electrophysiological properties, neurotransmitter types, and gene expression patterns. Such diversity not only ensures the precision and reliability of neural circuit functions but also provides the material basis for neural plasticity [4–6]. Recent technological advances in single-cell sequencing and optogenetics have enabled researchers to reveal the intrinsic nature of neural system heterogeneity more thoroughly, revolutionizing our understanding of the organizational principles of the brain [7].

Theoretical neuroscience has provided substantial insights into the computational advantages of neural heterogeneity. Gjorgjieva et al. [8] systematically investigated how the biophysical diversity of neurons and synapses influences circuit performance, demonstrating that temporal scale diversity significantly enhances network information processing capacity. Specifically, different combinations of time constants generate richer dynamical behaviors, providing a theoretical foundation for understanding the computational advantages of neural diversity. Complementing this work, Amit et al. [9] demonstrated that heterogeneity in neuronal parameters prevents networks from falling into pathological synchronization, thus increasing network resilience against noise.

These theoretical predictions have been extensively validated through experimental studies. Marder et al. [10] discovered that identical network functions can be achieved through multiple distinct combinations of ion channels, revealing that parametric heterogeneity provides the foundation for homeostatic plasticity. Building on this, Prinz et al. [11] found that parameters controlling network activity may exhibit considerable inter-animal heterogeneity, with various combinations of synaptic strengths and intrinsic membrane properties supporting proper network

* Corresponding author (email: wlin@fudan.edu.cn, xin.lu.lab@outlook.com)

© Science China Press 2026

performance. At the cellular level, Bean [12] revealed that individual neurons can express up to 20 different voltage-gated ion channels, enabling rich dynamical behaviors and explaining the mechanisms underlying diverse neuronal electrical activity. Nusser [13] combined electron microscopy with immunolabeling techniques to discover that ion channel subcellular localization displays precise spatial patterns, directly influencing synaptic integration and information processing.

A particularly significant manifestation of neural heterogeneity is bilateral lateralization, which has profound implications for specialized biological functions across diverse species. This lateralization (the asymmetrical distribution of neural structures and functions between the left and right hemispheres) represents a specialized form of heterogeneity that enhances neural processing efficiency through functional specialization [14, 15]. Drosophila has emerged as a powerful model organism for studying neural lateralization due to its relatively simple yet functionally sophisticated nervous system. Pascual et al. [16] documented in detail the asymmetrical body (AB) within the central complex, confirming that approximately 95% of wild-type Drosophila display a consistent lateralization pattern where the right AB is significantly larger than the left AB. This high population consistency suggests functional significance rather than random variation. Expanding on this structural foundation, Turner-Evans et al. [17] characterized the microstructural features of the asymmetrical body, revealing specialized neuronal groups with differential connectivity patterns between hemispheres. Beyond the central complex, Linneweber et al. [18] identified structural asymmetries in the Drosophila visual system, particularly in the R7/R8 photoreceptor projection regions, demonstrating these asymmetries result from programmed developmental processes.

Structure determines function [19–21]. Despite the widespread theoretical acceptance of neural heterogeneity as a concept, systematic investigations of neural structural heterogeneity based on authentic biological connectomes remain severely limited. Particularly regarding connectivity pattern heterogeneity, existing research is largely confined to specific brain regions or simplified models [3, 22], lacking comprehensive analyses of heterogeneity characteristics across complete neural networks. For example, while pronounced left-right asymmetries have been discovered in localized structures such as the AB and visual system [16], analyses of heterogeneity properties at the whole-brain network level, especially regarding symmetry and asymmetry patterns in global inter-hemispheric connectivity and spatial heterogeneity, remain virtually unexplored. This research gap primarily stems from the extreme difficulty in obtaining complete connectome data from biological organisms, with comprehensive connectomes currently available for only a few species [23]. This limitation has significantly impeded the ability to systematically analyze structural heterogeneity features embedded within biological connectomes and understand how these heterogeneity characteristics contribute to the functional diversity of neural systems.

With recent advances in connectomics technology, particularly the completion of the Drosophila connectome, researchers have the unprecedented opportunity to systematically investigate structural heterogeneity features and their potential functional significance in a complex biological neural system. Dorkenwald et al. [24] have mapped the adult Drosophila brain connectome with unprecedented detail, cataloging approximately 130000 neurons, over 50M synapses, and the positional morphology and functional classification of most neurons. This comprehensive dataset provides an exceptional foundation for exploring the complexity of biological neural systems.

Existing analyses of this connectome have established foundational statistical properties, including degree distributions, connection weights, and community structure [25]. Recent studies have further examined recurrent cores and super-hub organization in the Drosophila connectome [26], as well as the interaction between network topology and temporal or spiking dynamics [27]. However, several important questions remain unexplored. First, how does structural heterogeneity manifest simultaneously in network topology and spatial organization, and how do these two dimensions relate to each other? Second, to what extent is the Drosophila brain bilaterally symmetric at the structural level, and can this symmetry be distinguished from a trivial byproduct of degree distributions? Third, if structural symmetry prevails, what mechanism drives functional lateralization between hemispheres? In this study, we address these questions through four specific contributions: (1) a joint network-spatial characterization of structural heterogeneity, complemented by rigorous statistical testing of the degree and weight distributions, including power-law model selection against alternative heavy-tailed distributions using the Clauset-Shalizi-Newman framework; (2) a quantitative assessment of bilateral symmetry via the earth mover's distance metric, validated by a cross-region null model that demonstrates homologous left-right region pairs are significantly more similar than non-homologous pairs; (3) a dynamical analysis using the Kuramoto model revealing that functional asymmetry arises from the interplay of intrinsic frequency differences and structured inter-hemispheric connectivity, the former serving as the primary driver and the latter as an amplifier of stimulus-induced lateralization, as confirmed by a degree-preserving edge-swap control experiment; and (4) a systematic comparison of spatial versus network-topological features for neuronal type clustering, demonstrating that spatial proximity outperforms pure connectional fingerprints in recapitulating expert-annotated cell types.

The visualization of the Drosophila brain network constructed in this study is demonstrated in Figure 1.



Figure 1 (Color online) Visualization of the Drosophila brain network.

2 Results

2.1 Structural heterogeneity

The Drosophila brain consists of a vast network of neurons engaged in complex interactions, which collectively define its structural complexity. In this section, we characterize the statistical properties of the Drosophila brain network at both global and regional scales, demonstrating the heterogeneous nature of network nodes and their associated connectivity patterns.

2.1.1 *Multi-dimensional heterogeneity in the global structure*

The degree distribution of neurons in the Drosophila brain network follows a power-law pattern (Figure 2(a)). The median and mean degrees are 20 and 37.01, respectively. Notably, only 7.35% of neurons have more than 100 synaptic connections, and a mere 0.076% exhibit degrees exceeding 1000. In general, higher in-degree, which is defined as the number of afferent synaptic inputs received from presynaptic partners, is positively correlated with higher out-degree, i.e., the number of efferent projections sent to postsynaptic targets (Pearson's $r = 0.766$; Figure 2(b)). Moreover, node degree and node strength are strongly correlated (Pearson's $r = 0.95$, $p < 0.001$), following a power-law relationship: as the degree increases, the node strength also increases accordingly (Figure 2(c)). Similarly, the distribution of connection weights follows a power-law, indicating that while a small subset of neuron pairs are connected by a large number of synapses, most exhibit relatively few connections (Figure 2(d)). The mean connection weight is 12.6, suggesting that, on average, connected neuron pairs share approximately 12.6 synapses. Together, these results highlight the pronounced heterogeneity of the network at the global level.

Notably, although node degree and node strength are strongly correlated, the weight information is not redundant. Node strength S_i (defined in Subsection 3.2.5 as the sum of synaptic weights across all incident edges) and node degree measure different aspects of connectivity: neurons with identical degrees can have substantially different total synaptic weights due to variation in synapse counts per connection. Furthermore, connection weights range over several orders of magnitude (Figure 2(d)), providing an independent dimension of heterogeneity beyond degree alone. Thus, degree and weight jointly capture complementary facets of network connectivity.

To rigorously test whether the observed degree and connection-weight distributions follow power-law behavior, we applied the Clauset-Shalizi-Newman framework [28] using maximum-likelihood estimation, KS-based goodness-of-fit tests (semi-parametric bootstrap, $n = 200$–1000), and likelihood-ratio tests against four alternative heavy-tailed distributions (exponential, log-normal, stretched-exponential, and truncated power-law). For the degree distribution (Figure 3(a)), the power-law fit is not rejected (KS $p = 0.094$, $\alpha_k \approx 2.99$, $k_{\min} = 143$), but log-normal and truncated power-law are statistically indistinguishable alternatives. For the edge-weight distribution (Figure 3(b)), the KS

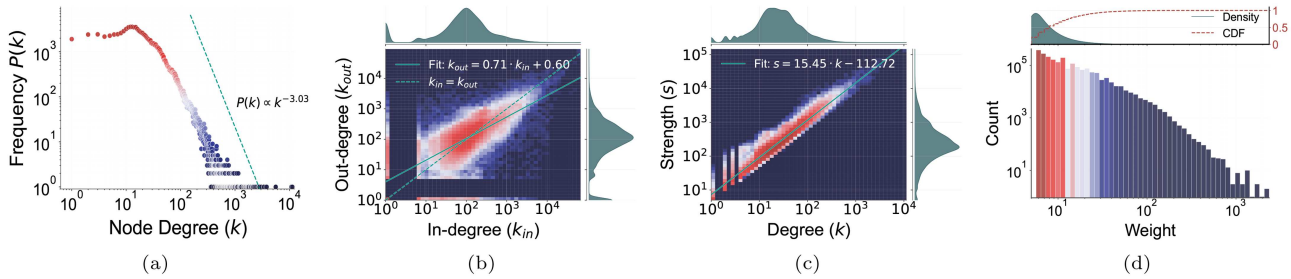

Figure 2 (Color online) Statistical properties of the Drosophila brain network. (a) Degree distribution of the Drosophila brain network. (b) Correlation between in-degree and out-degree. The red line denotes the reference values, whereas the green line represents the fitted curve. (c) Relationship between node degree and node strength. (d) The distribution of connection weights. Here, we revisit these statistics using the raw connectome with a preprocessing procedure that differs from previous studies [25] (see methods).

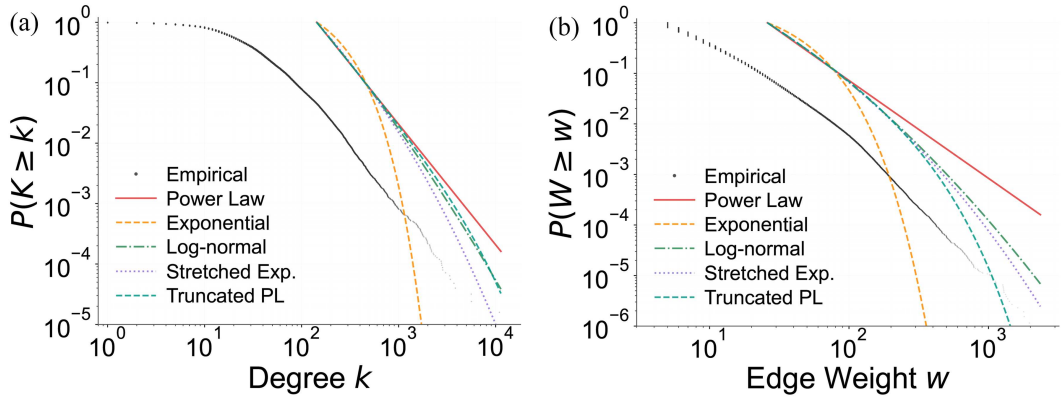

Figure 3 (Color online) Power-law and alternative heavy-tailed distribution fits. (a) Degree distribution CCDF with five candidate distributions. (b) Edge-weight distribution CCDF with five candidate distributions. The power-law (red dashed) provides an acceptable KS fit in both cases, but log-normal (green) is statistically preferred for edge weights by likelihood-ratio tests.

test does not reject the power-law ($p \approx 1.0$, $\alpha_w \approx 2.93$, $w_{\min} = 26$); however, likelihood-ratio tests reveal that log-normal, stretched-exponential, and truncated power-law all provide significantly better fits (all $p < 10^{-3}$). These results confirm that both distributions are heavy-tailed, but strict power-law behavior receives only partial support, particularly for edge weights, where log-normal is the preferred model.

2.1.2 *Structural heterogeneity and bilateral symmetry in functional regions*

The nervous systems of most organisms, including Drosophila, are divided into functional regions, each with specialized characteristics in structure and function. Investigating the heterogeneity of these regions offers valuable insights into the organizational principles and complexity of the nervous systems. In this section, we quantify the neurons' numbers, synaptic densities, and inter-region synaptic connectivity within distinct anatomical areas to investigate the heterogeneity among different functional regions.

The neuronal distribution across various regions reveals that vision-related neurons constitute the largest proportion (Figure 4(a)). We initially report the heterogeneity across various functional regions with respect to the number of neurons they contain. Specifically, neurons associated with optic and visual projection areas collectively represent 71.06% of the total number of neurons. Furthermore, the neuronal counts exhibit a relatively symmetrical distribution between the left and right hemispheres across most regions. The most pronounced hemispheric heterogeneity is observed in the visual (sensory) region, where the neuronal population differs by approximately 37.50% between the left and right hemispheres.

In addition, we analyzed the quantity of connections within each region. Figure 4(b) depicts the histogram of synaptic connections, defined as all neuronal interconnections within the boundaries of each analyzed region. Consistent with the neuronal distributions, vision-related regions exhibit the highest synaptic counts, accounting for 80.11% of the total intra-regional synapses. Notably, the number of synapses maintains a high degree of bilateral symmetry across regions. The most pronounced heterogeneity is observed in the gustatory region, where the inter-hemispheric difference in synaptic density approximates 29.41% of the total synapses within this region. Furthermore, we analyzed the number of connections between regions. It is evident that numerous regions exhibit

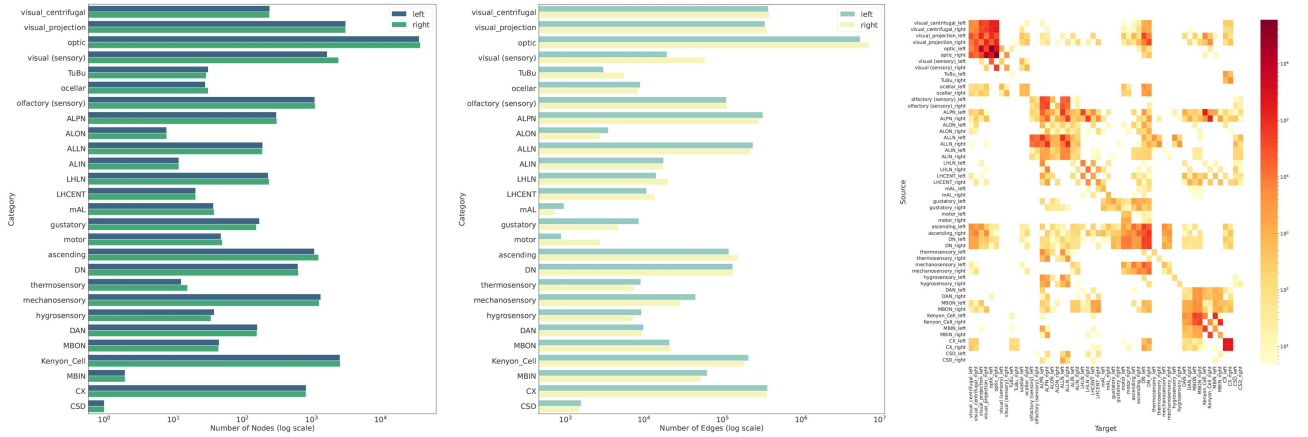

(a) (b) (c)

Figure 4 (Color online) The number of neurons and synaptic densities within distinct anatomical regions. (a) The number of neurons across distinct regions of the Drosophila connectome; (b) the synaptic density within each region; (c) heat map of the inter-regional synaptic connectivity patterns.

a pronounced small-world phenomenon, exemplified by notable clustering effects among areas associated with visual (visual_centrifugal, visual_projection, optic, visual (sensory), TuBu, and ocellar), olfactory (olfactory (sensory), ALPN, ALON, ALLN, and ALIN), and learning and memory functions (DAN, mushroom body output neuron (MBON), Kenyon cell, and MBIN) (Figure 4(c)). Concurrently, we calculated the ratio of intra-regional to inter-regional connections, finding that the magnitude of intra-regional connections is approximately 23.48 times greater than that of inter-regional connections. The results demonstrate pronounced heterogeneity in neuronal connectivity patterns both within and between functional regions. Specifically, intra-regional connections exhibit remarkably high density, whereas inter-regional connections are notably sparse, which is consistent with previous studies [29]. Furthermore, regions with similar functions display a higher number of synaptic connections between them, indicating significant heterogeneity in inter-regional connection strength. Moreover, this study observed functional segregation between many functionally distinct areas. For instance, internal connections within visual processing regions constitute 98.96% of the total connections in these areas. Concurrently, internal connections within olfactory processing regions represent 73.98% of the total connections in those regions.

To further investigate the heterogeneity of inter-regional statistical characteristics, we conceptualized regions as subgraphs and analyzed the statistical distributions of these subgraphs (Figure 5), including degree distribution, clustering coefficient, and betweenness centrality. The regions with the highest average degree are ALLN and CX (with an average degree of approximately 50), while the remaining regions exhibit average degrees not exceeding 30 (Figure 5(a)). In addition, the internal in-degree and out-degree distributions within these regions are approximately equivalent (Figures 5(b) and (c)). Figures 5(d) and (e) illustrate the clustering coefficients for directed and undirected networks among regions, respectively. The results show minimal disparity between the clustering coefficients of directed and undirected networks, suggesting a predominance of bidirectional connections among neurons (i.e., neuron A can transmit signals to neuron B, and vice versa). The mean betweenness centrality coefficients for each region are generally low, consistent with the overall network distribution (Figure 5(f)). However, the MBON region stands out with a significantly higher mean betweenness centrality. MBONs are the primary efferent neurons of the mushroom body, which is critical for learning, memory, and behavioral output in Drosophila. The elevated betweenness centrality of MBONs suggests that they serve as key nodes linking multiple functional areas, likely playing a crucial role in transmitting processed information to other regions. Their high centrality may also reflect their involvement in translating learning and memory outcomes into behavioral responses, underlining their importance in coordinating complex behavioral patterns.

In order to further examine the similarity between homologous subregions across the left and right hemispheres, we computed and visualized the degree distributions for each cortical region (Figure 6). To quantify the interhemispheric similarity of these distributions, we employed the earth mover's distance (EMD, see data and methods) metric, normalized to account for potential variations in distribution scale. Specifically, we calculated the normalized EMD similarity coefficient between the left and right hemisphere distributions for each region. Our results demonstrate that an overwhelming majority of regions exhibit remarkably low EMD similarity coefficients. This finding strongly suggests a high degree of concordance in the degree distributions between homologous regions in the left and right hemispheres. Such bilateral symmetry in network topology may have significant implications for

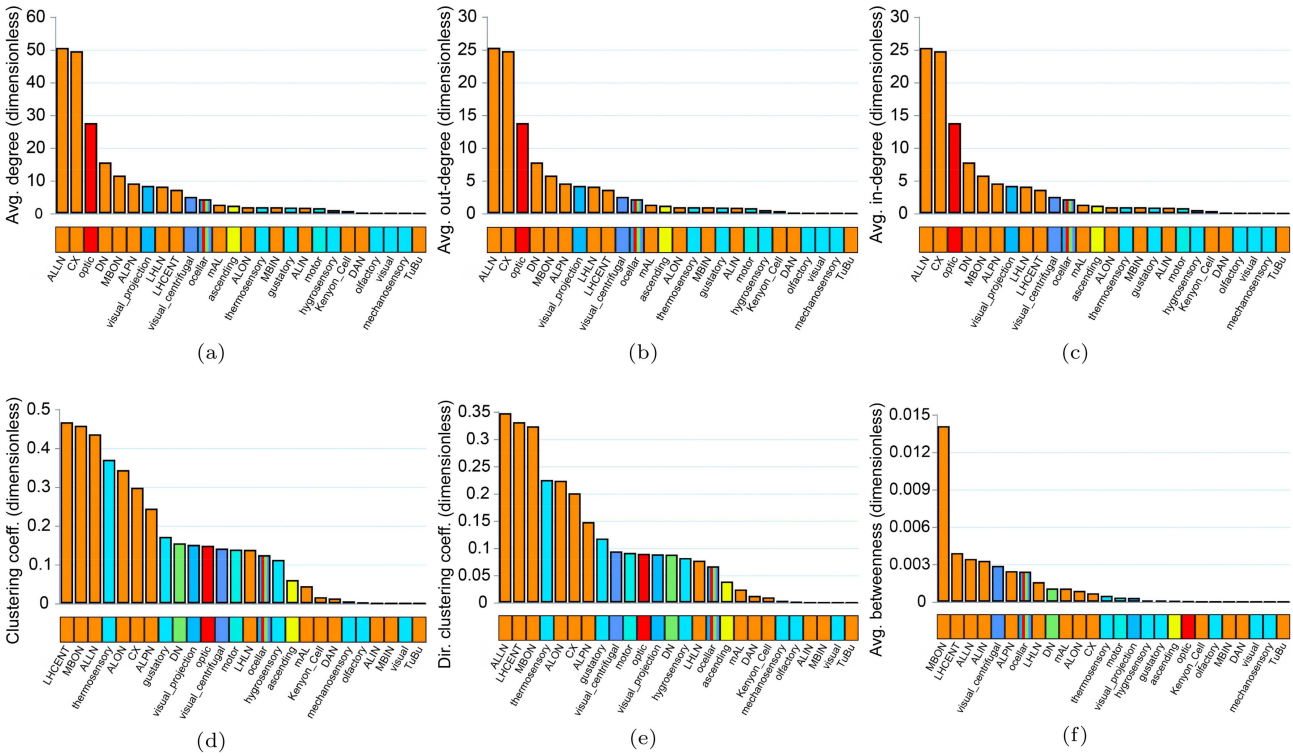

Figure 5 (Color online) Statistical distribution of networks composed of regions. (a) The average degree across various regions; (b) the average out-degree for the respective regions; (c) the average in-degree for each region; (d) the clustering coefficient for each region (undirected graph); (e) the average directed clustering coefficient across regions; (f) the average betweenness centrality coefficient for the regions.

our understanding of brain organization and function. Note that the visual (sensory) and MBIN regions exhibit a relatively high EMD coefficient, indicating substantial asymmetry in the degree distribution of visual input neurons between the left and right hemispheres of the brain.

To formally assess whether the observed bilateral symmetry exceeds chance-level expectation, we designed a cross-region permutation test. For each region X, the homologous EMD $\mathrm{EMD}(L_X, R_X)$ was compared against a null distribution constructed by repeatedly pairing L_X with randomly sampled non-homologous right hemispheres R_Y ($Y \neq X$, 10000 draws). The raw p-value was defined as the fraction of random pairings whose EMD is smaller than or equal to the homologous EMD, with Bonferroni correction applied across all tested regions. Critically, for no region was the homologous EMD significantly larger than the null, meaning that homologous left-right pairs were never less similar than random cross-region pairings. This indicates a consistent, unidirectional trend toward bilateral symmetry across the entire connectome. Among the 26 regions tested, 14 achieved $p_{\mathrm{raw}} < 0.05$ and 13 survived Bonferroni correction ($p_{\mathrm{bonf}} < 0.05$), providing positive statistical evidence for bilateral symmetry in these regions. The remaining 12 regions did not reject the null hypothesis and are therefore not significantly asymmetric; several of these (e.g., MBIN) contain very few neurons, indicating that their non-significance may reflect insufficient sample size rather than a genuine absence of bilateral symmetry. Taken together, these results indicate that the bilateral similarity between homologous left-right region pairs is a specific organizational feature of the connectome, not a trivial consequence of degree distributions.

2.2 Spatial clustering and functional organization

The spatial distribution and clustering patterns of neurons are analyzed and visualized in Figure 7. As shown in Figure 7(a), the 3D kernel density estimation (KDE) scatter plot and the nearest neighbor distance histogram reveal a nearest neighbor index ($R = 0.54$), indicating a significant deviation from random spatial distribution and reflecting an overall agglomerative pattern. In the left and right hemispheres, 3D KDE scatter plots (Figures 7(b) and (c)) reveal R values of 0.46 and 0.50, respectively, suggesting notable hemispheric differences in neuronal clustering. Regional analysis, as depicted in Figure 7(d), shows that most brain regions have R values lower than the whole-brain average, implying that neurons with similar functions tend to cluster within specific anatomical areas.

Interestingly, mushroom body input neurons (MBINs) exhibit a markedly dispersed distribution, with an R

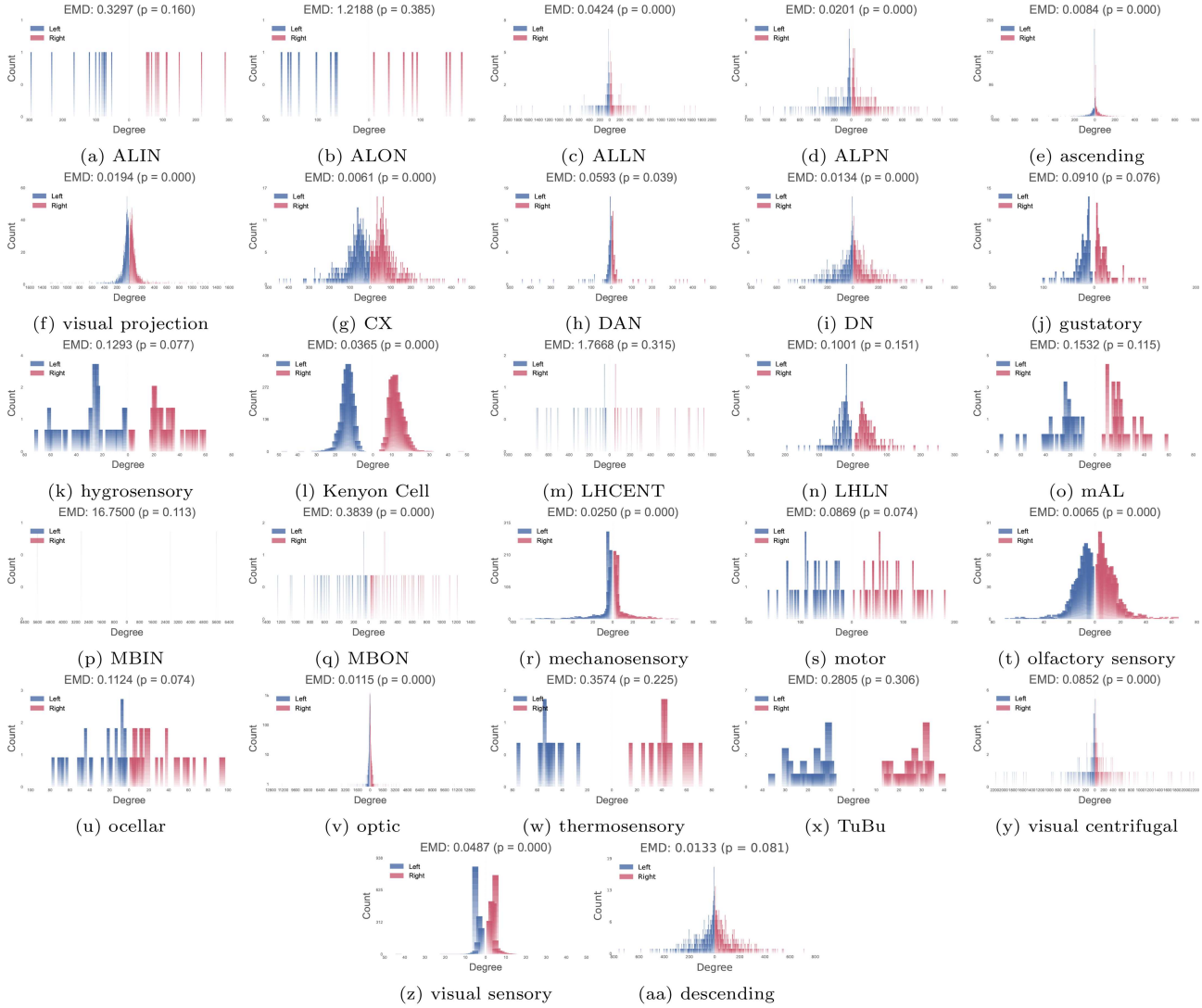

Figure 6 (Color online) Degree distributions of left and right hemispheres across diverse regions.

value of 2.99. This unusual spatial pattern may be attributed to their functional role in transmitting sensory information and internal state signals to the mushroom body. Such a function requires widespread anatomical coverage, enabling MBINs to integrate inputs from multiple sensory modalities and distributed brain regions. This dispersed arrangement likely facilitates the efficient collection and integration of information necessary for the modulation of complex behaviors governed by the mushroom body.

Moreover, significant disparities in the distribution of neurons between the left and right hemispheres in specific regions, notably ALIN, ALON, Kenyon cells, and tubercle bulb (TuBu) neurons, were observed (Figure 7(d)). This hemispheric asymmetry may be attributed to several factors. First, certain brain regions may have distinct functional roles in the left and right hemispheres, resulting in differential neuronal distributions. This functional lateralization could be associated with specific cognitive processes or behavioral outputs. Second, the observed asymmetry in neuronal distribution between hemispheres may reflect divergent information processing strategies or optimizations in computational efficiency. Such differences could potentially enhance the overall processing capacity and flexibility of the Drosophila brain [30].

In order to further examine the spatial distribution patterns across specific functional regions, we present spatial clustering images for all regions (Figure 8). These images elucidate the intra-regional variations in spatial agglomeration and spatial concentration patterns. All regions exhibited significant spatial agglomeration patterns, indicating that neurons within the same functional region demonstrate a strong tendency for spatial clustering. The spatial agglomeration is quantified by the nearest neighbor index R (see Subsection 3.3 for definition), where $R < 1$ indicates spatial clustering and $R > 1$ indicates dispersion. For each region, we present a 3D KDE scatter

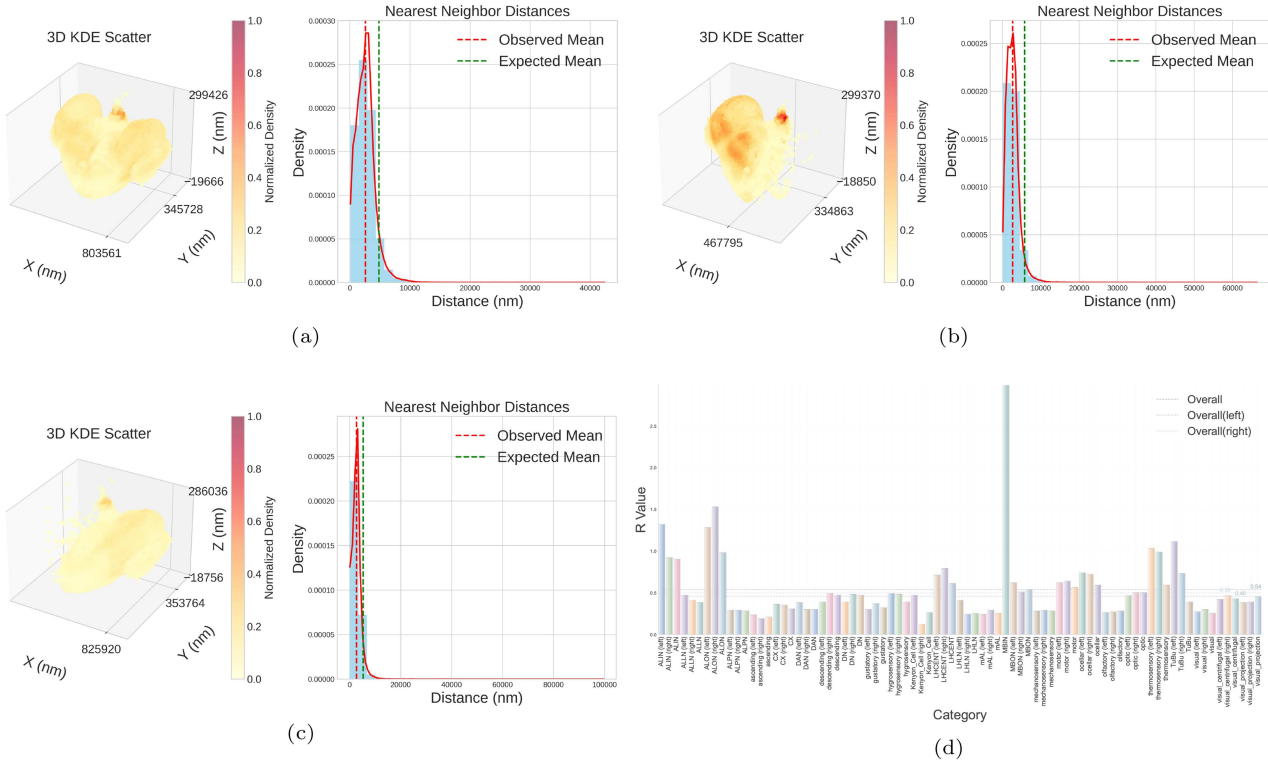

Figure 7 (Color online) Spatial distribution and clustering analysis of neuronal somata. The spatial distribution of neurons and the distribution of nearest neighbor distances for the (a) entire brain, (b) left hemisphere, and (c) right hemisphere, respectively; (d) the nearest neighbor index R for regions. Each bar represents a specific brain area, with the bar height indicating the R value for that region.

plot that visualizes the spatial density of neuronal somata, with warmer colors representing higher local neuron density. Each subfigure also includes a histogram of nearest neighbor distances, which provides a complementary quantitative view: a left-shifted histogram (toward shorter distances) corroborates strong spatial clustering, whereas a more spread-out distribution toward longer distances indicates greater dispersion. The 3D KDE maps reveal that the spatial organization varies considerably across regions. For instance, Kenyon cells (intrinsic neurons of the mushroom body) show a highly concentrated distribution pattern reflecting their densely packed arrangement in the mushroom body calyx, while MBINs exhibit a more dispersed pattern ($R = 2.99$; Figure 7(d)), consistent with their functional requirement to collect sensory information from broadly distributed brain areas. However, notable heterogeneity in spatial aggregation was observed between bilateral hemispheres, particularly in the hygrosensory, Kenyon cell, and thermosensory regions. This inter-hemispheric variation in spatial clustering may reflect subtle developmental differences or functional asymmetries between the left and right hemispheres, and warrants further investigation in future studies.

Further, to investigate the correlation between the pervasive spatial clustering observed in cerebral networks and neuronal typology, we implemented the K-means clustering [31], spectral clustering [32], and hierarchical clustering algorithm [33] to categorize the entire neuronal population into 58 distinct clusters, corresponding to the total number of identified neuronal types. Figure 9 presents a comparative analysis between the outcomes of spatial clustering algorithms applied to the entire neuronal population and the actual neuronal classifications. Figures 9(a) and (b) elucidate the inefficacy of spatial clustering algorithms in effectively partitioning diverse neuronal types. These results underscore the inadequacy of relying solely on spatial attributes for neuronal type discrimination.

To further assess whether spatial proximity or network topology better accounts for neuronal identity, we compared three feature representations for K-means clustering (k = number of true cell types): (1) spatial coordinates (xyz), (2) spectral embedding of the directed adjacency matrix (truncated SVD, top-k left and right singular vectors), and (3) combined spatial and spectral features. Clustering quality was evaluated by normalized mutual information (NMI) and adjusted rand index (ARI) against expert-annotated cell type labels, with significance assessed via permutation tests (1000 iterations). As summarized in Table 1, spatial features achieved the highest NMI (0.29) and ARI (0.04), while spectral embedding yielded a lower NMI (0.25) and a negative ARI (-0.03, $p = 1.0$), indicating no concordance with annotated cell types beyond random assignment. Combining spatial and spectral features did not improve performance (NMI = 0.26, ARI = 0.01). These results indicate that neuronal identity

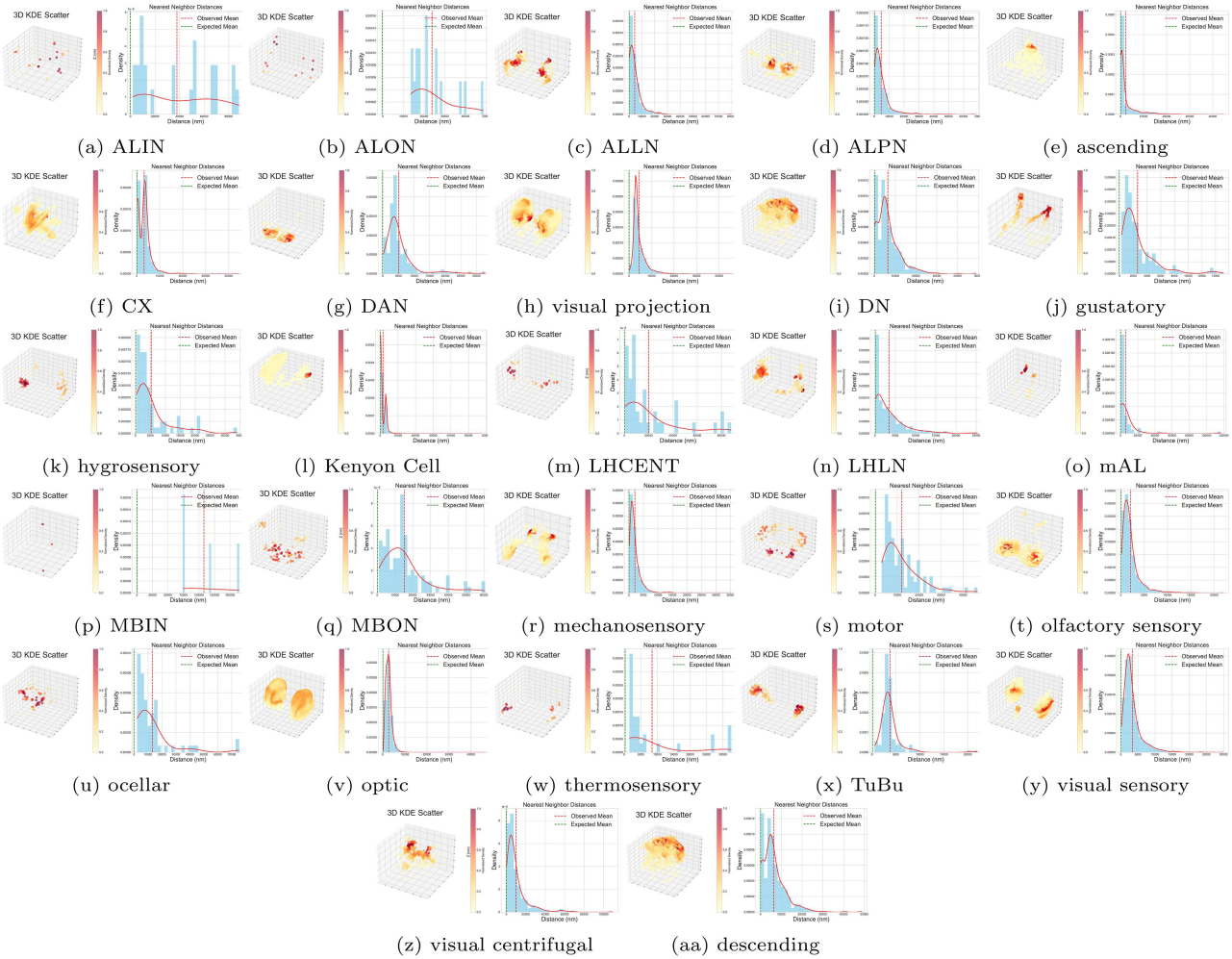

Figure 8 (Color online) Spatial agglomeration patterns across diverse regions.

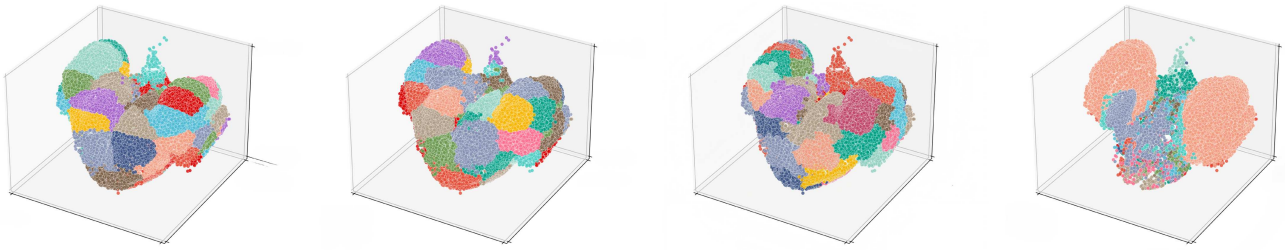

Figure 9 (Color online) Comparative analysis of spatial clustering and neuronal typology. The outcomes of spatial clustering analysis using (a) K-means, (b) spectral clustering, and (c) hierarchical clustering, respectively, segregating neurons into 58 distinct categories that numerically correspond to the established neuronal classifications; (d) the results of neuronal classification, employing a color-coded scheme to differentiate various neuronal subtypes.

in the current connectome annotation is more closely associated with spatial location than with pure connectional fingerprint, consistent with the view that cell type definitions integrate multiple modalities, including morphology, neurotransmitter profile, and developmental lineage, which goes beyond connectivity alone.

2.3 Validation of hemispheric functional heterogeneity

As a form of heterogeneity, previous analyses have reported structural symmetry in the left and right parts of the Drosophila brain, yet numerous studies have demonstrated functional asymmetry [34,35] in neuronal systems. One

Table 1 Clustering performance of spatial, spectral, and combined features against expert-annotated cell types.

Method	NMI	NMI p	ARI	ARI p
Spatial (xyz)	0.2920	<0.01	0.0436	<0.01
Spectral (SVD)	0.2478	<0.01	−0.0319	1.000
Combined	0.2613	<0.01	0.0074	<0.01

hypothesis addressing functional heterogeneity suggests that neurons in the left and right hemispheres demonstrate intrinsic differences in their functional patterns [34]. To test this hypothesis, we employed the Kuramoto model (for details, please refer to Subsection 3.6) to simulate neuronal activity, where the intrinsic frequencies of neurons in the left and right hemispheres were initialized using Gaussian distributions with distinct means and variances. The specific frequency parameters (μ and σ) used here serve as illustrative values to probe the qualitative effect of inter-hemispheric frequency heterogeneity; the absolute values are not intended to correspond to specific electrophysiological measurements. In the Kuramoto model, it is the relative difference in frequency distributions between hemispheres—rather than the absolute frequencies—that governs the emergence of synchronization asymmetry. Our qualitative conclusions hold as long as one hemisphere exhibits greater frequency dispersion than the other. Following random initialization, we conducted iterations over an extended time period and recorded the temporal evolution of the synchronization rate.

Notable differences in synchronization rates (R) emerge (Figure 10). Specifically, at $\lambda = 10000$ and $t = 25$ ms, the synchronization rates for the left and right hemispheres are 0.765 (Figure 10(c)) and 0.532 (Figure 10(e)), respectively. Similarly, at $\lambda = 2000$ and $t = 25$ ms, the synchronization rates are 0.059 and 0.233, and at $\lambda = 5000$, they are 0.273 and 0.615. These results indicate that for each hemisphere, a higher mean variance impedes its own synchronization capability, consequently leading to differences in overall activation levels (Figures 10(d) and (f)).

Despite the relatively similar network structures between the left and right hemispheres (Figure 6), subtle structural disparities persist. Consequently, whether these architectural distinctions between hemispheric networks potentially contribute to differential synchronization rates between the left and right hemispheres remains an unresolved question warranting further investigation.

Accordingly, we investigated functional lateralization differences between the left and right hemispheres by maintaining identical intrinsic frequencies of neurons across both hemispheres while employing differential input signals, thereby examining hemispheric functional asymmetries in response to varied input conditions. The intrinsic frequencies of all neurons were initialized using Gaussian distributions with identical means (0.1) and standard deviations (0.1), and their initial phases were assumed to follow uniform distributions ranging from 0 to 2π. On this basis, we recognized all 270 ocellar retinula cells and adjusted their frequencies to simulate instantaneous frequency changes when neurons receive external stimulation (ocellar-type neurons, which are part of visual input neurons). These neurons respond to light stimuli and are activated relatively early in the visual processing of Drosophila. We conducted iterations over an extended time period and recorded changes in synchronization rates between left and right hemispheres. Considering that different neurons receive varying light intensities depending on their angles, we established a maximum activation frequency and adjusted the activation frequencies of stimulated neurons to any value between their intrinsic frequency and the maximum activation frequency.

The average temporal evolution of synchronization rates between the left and right hemispheres across 10 experiments Figure 11 presents the temporal evolution of synchronization in the left and right hemispheres under four stimulation conditions, averaged over 10 simulation runs for each condition. Underall conditions, synchronization in bothh emispheres increases over time and gradually approaches a plateau during the later stages of the simulation.

At 150 ms, the differences in activation rates between the two hemispheres are consistently small, with values of 0.032, 0.032, 0.031, and 0.032 in Figures 11(a)–(d), respectively. These results suggest that external stimulation alone, without corresponding intrinsic frequency differences, produces only modest inter-hemispheric synchronization divergence.

To further test whether structural connectivity patterns contribute to functional asymmetry beyond intrinsic frequency differences, we performed a degree-preserving edge-swap control experiment. A randomized network was constructed by applying 100% degree-preserving directed edge rewiring to the original connectome, preserving each neuron's in-degree and out-degree while destroying the specific inter-region and inter-hemispheric wiring patterns. We then repeated the four-condition ocellar stimulation protocol (center, left, right, all) on this randomized network, with identical intrinsic frequency distributions in both hemispheres. Figure 12 compares the left-right synchronization asymmetry $\Delta R_{LR} = |R_L - R_R|$ between the original and edge-swap networks. In three of four stimulation conditions (center, left, and all), the edge-swap network exhibited significantly *smaller* inter-hemispheric

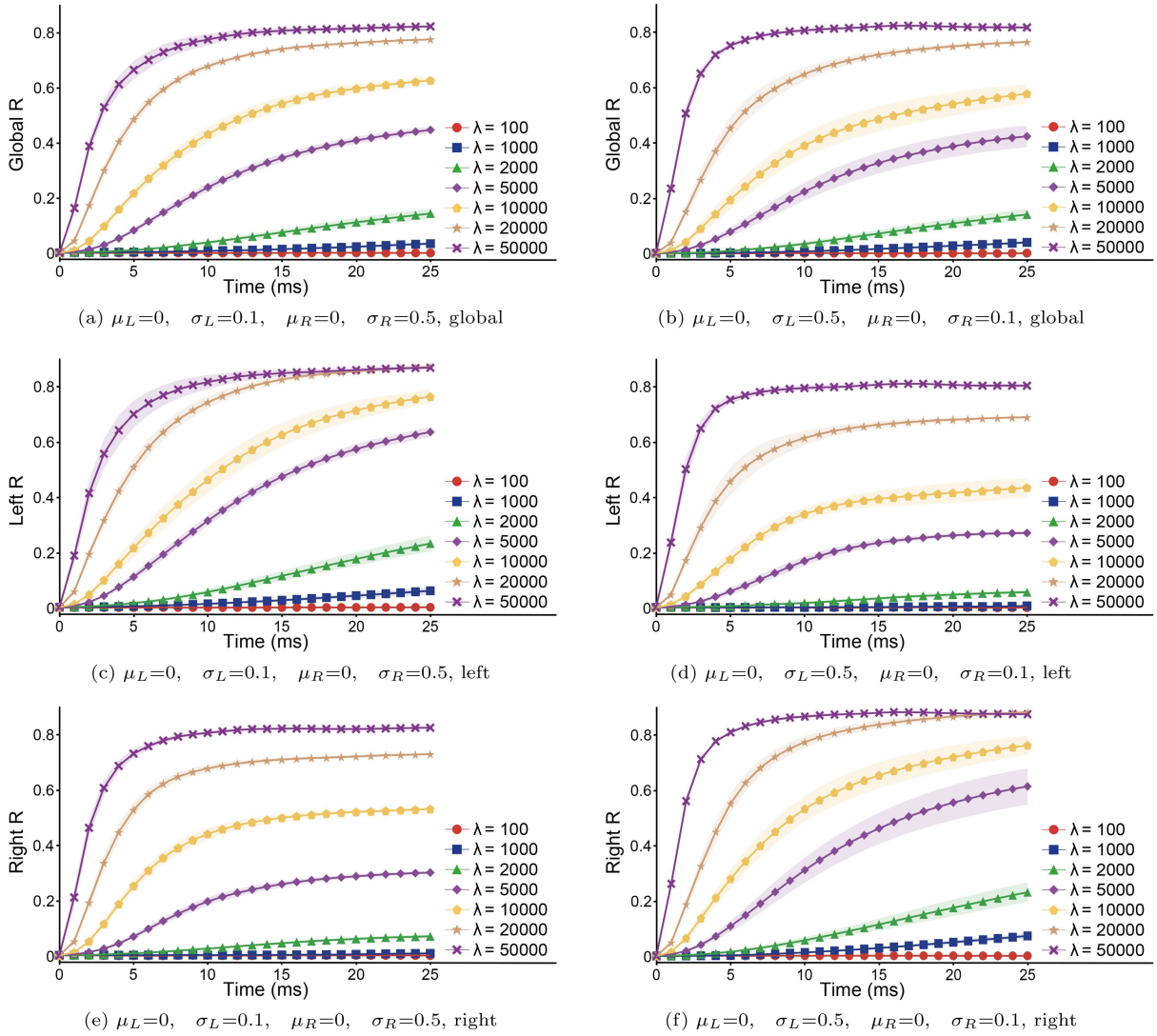

(a) μ_L=0, σ_L=0.1, μ_R=0, σ_R=0.5, global

(b) μ_L=0, σ_L=0.5, μ_R=0, σ_R=0.1, global

(c) μ_L=0, σ_L=0.1, μ_R=0, σ_R=0.5, left

(d) μ_L=0, σ_L=0.5, μ_R=0, σ_R=0.1, left

(e) μ_L=0, σ_L=0.1, μ_R=0, σ_R=0.5, right

(f) μ_L=0, σ_L=0.5, μ_R=0, σ_R=0.1, right

Figure 10 (Color online) Temporal evolution of synchronization rates for the whole brain, left hemisphere, and right hemisphere under different initialization parameters. The time step $\delta_t = 0.05$ ms with a simulation period $T = 25$ ms. Neural oscillator frequencies are characterized by μ_L, σ_L (mean and standard deviation (S.D.) for left hemisphere) and μ_R, σ_R (mean and standard deviation (S.D.) for right hemisphere).

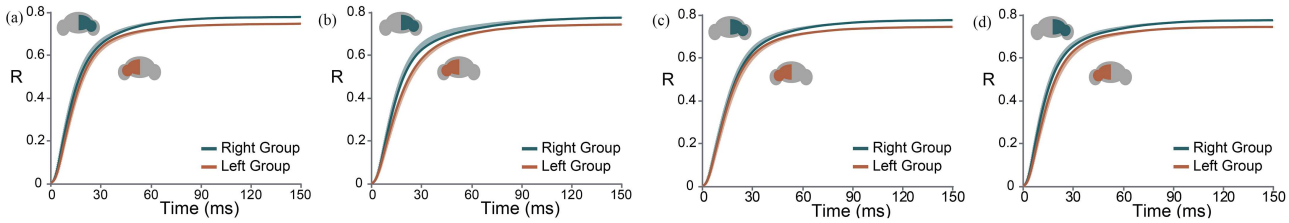

Figure 11 (Color online) Temporal evolution of left-right brain synchronization rate (R) during external stimulation of optic superclass ocellar-type neurons. We set coupling strength $\lambda = 5000$, time step $\delta_t = 0.25$ ms, simulation period $T = 150$ ms. The temporal evolution of left-right brain synchronization rate (R) when stimulating ocellar-type neurons exclusively in the (a) central brain, (b) left brain, (c) right brain, and (d) all ocellar-type neurons, respectively.

asymmetry than the original network ($p < 0.01$ for center and all, $p < 0.05$ for left). This indicates that the specific wiring patterns of the biological connectome *amplify* stimulus-driven functional asymmetry: unilateral stimulation propagates through structured inter-hemispheric pathways, producing a measurable left-right divergence. When these pathways are randomized, the stimulation effect diffuses more uniformly across both hemispheres, attenuating the asymmetry. This finding confirms that structural connectivity makes an independent contribution to functional lateralization. However, the magnitude of this structural effect, in which the edge-swap network reduces ΔR_{LR}

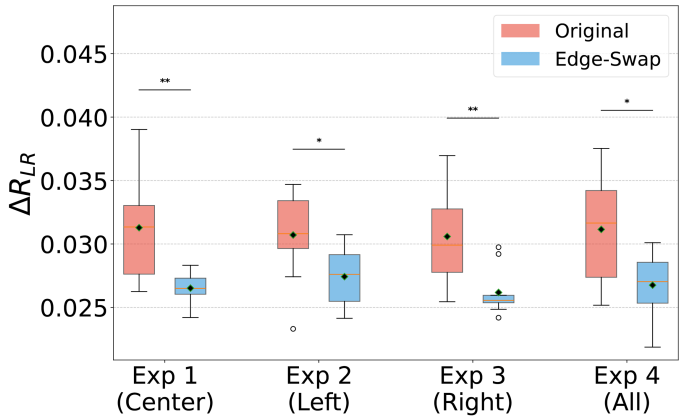

Figure 12 (Color online) Left-right synchronization asymmetry comparison between the original connectome and the degree-preserving edge-swap null network. Boxplots show the distribution of $|R_L - R_R|$ at steady state ($t = 150$ ms) across 10 repeated simulations under four ocellar stimulation conditions.

from approximately 0.03 to an even smaller value, is far smaller than the asymmetry produced by intrinsic frequency differences (ΔR_{LR} on the order of 0.2; Figure 10). This comparison reveals a clear hierarchy: frequency heterogeneity is the dominant driver of functional lateralization, while structured inter-hemispheric connectivity plays a secondary, modulatory role.

3 Data and methods

3.1 Drosophila connectome data

We utilized the largest recently released Drosophila brain connectome [24], which represents the first complete connectome of an adult Drosophila brain. It encompasses approximately 130000 reconstructed neurons and over 50M mapped chemical synapses, covering the central, afferent, and efferent neurons. Neuron type annotation in this dataset mainly comes from expert knowledge. The annotation process is designed to be dynamic and continuously updated, allowing for the incorporation of new research findings. This comprehensive approach also features detailed synaptic connections and high-precision 3D coordinates (accurate to the nanometer level) for both cell bodies and synapses. For more detailed information, please refer to [24, 36].

In this study, we utilized the raw connectome data without applying any additional filtering or preprocessing procedures, such as synapse count thresholds or confidence-based pruning. This decision was motivated by the goal of preserving the full complexity of the biological connectivity patterns, including weak connections that may carry functionally relevant information. While the companion network analysis by Lin et al. [25] applied a threshold of five synapses per connection to construct a simple directed graph, our approach retains all synaptic connections and represents the network as a directed multigraph, thereby capturing the complete spectrum of connection strengths between neuronal pairs. Notably, the vast majority of neurons (over 98%) belong to the giant weakly connected component, indicating that potential isolated neurons constitute a very small fraction of the dataset and would not affect the overall statistical properties reported in this study.

3.2 Network analysis metrics

3.2.1 *Graph definition*

In the Drosophila connectome dataset, multiple directed connections may exist between neurons. To accurately represent this complex connectivity pattern, we employ a directed multigraph model to describe this dataset.

A directed multigraph G is defined as an ordered pair $G = (V, E)$. Here, let V represent a set of vertices, also known as nodes, which are the fundamental units of the network. Let E, on the other hand, be a set of ordered pairs of nodes, called directed edges or arcs. These edges represent the connections or relationships between the nodes, with the direction indicating the nature of the relationship. In a multigraph, multiple edges are allowed between the same pair of nodes, which can represent different types of relationships or interactions. In this paper, we represent neurons as nodes and synaptic connections between neurons as edges.

Throughout this study, different analyses employ the graph representation most appropriate to the question at hand. All network-level statistical characterizations (including degree distributions, connection weight distributions,

bilateral symmetry quantification via EMD, and the cross-region permutation test) use the full directed multigraph, with node degree defined as the total number of incident synapses. For the power-law model selection analysis (Subsection 2.1.1), the edge-swap null network (Subsection 2.3), and the spectral embedding for neuronal type clustering (Subsection 2.2), we work with the underlying simple directed graph, where multiple synapses between the same neuron pair are deduplicated to a single binary connection. In all cases, edge direction is preserved and no synapse-count threshold is applied.

3.2.2 *Degree*

The degree of a node is a fundamental measure of its connectivity in a graph. In a directed graph, we distinguish between two types of degree for a node v. The out-degree, denoted as $d^+(v)$, is the number of edges that originate from vertex v and is formally defined as $d^+(v) = |\{(v,u) \in E, u \in V\}|$. This measures the number of connections that v initiates with other vertices. Conversely, the in-degree, denoted as $d^-(v)$, is the number of edges that terminate at vertex v and is defined as $d^-(v) = |\{(u,v) \in E, u \in V\}|$. This measures the number of connections that other vertices initiate with v. The total degree of a vertex is the sum of its in-degree and out-degree, that is

$$d(v) = d^+(v) + d^-(v). \tag{1}$$

These measures provide insights into the importance or centrality of a node in the network.

3.2.3 *Clustering coefficient*

The clustering coefficient is a measure of the degree to which nodes in a graph tend to cluster together. It provides insights into the local structure of networks and is often used to identify tightly-knit groups within the network.

Undirected networks. For undirected networks, the local clustering coefficient for a node i with k_i neighbors is defined as

$$C_i = \frac{2|\{e_{jk} : v_j, v_k \in N_i, e_{jk} \in E\}|}{k_i(k_i-1)}, \tag{2}$$

where N_i is the neighborhood of vertex i. This coefficient represents the fraction of pairs of i's neighbors that are connected to each other, indicating how close the vertex and its neighbors are to forming a clique.

Directed networks. In directed networks, the local clustering coefficient for a node i is calculated as

$$C_i = \frac{|\{e_{jk} : v_j, v_k \in N_i, e_{jk} \in E\}|}{k_i(k_i-1)}. \tag{3}$$

This definition takes into account the directionality of the edges, providing a more nuanced measure of clustering in directed graphs.

Weighted networks. For weighted networks, the clustering coefficient is adapted to incorporate edge weights. The weighted clustering coefficient for a vertex i is defined as

$$C_i^w = \frac{1}{s_i(k_i-1)} \sum_{j,k} \frac{(w_{ij}+w_{ik})}{2} a_{ij}a_{ik}a_{jk}, \tag{4}$$

where s_i is the strength of vertex i, k_i is its degree, w_{ij} is the weight of the edge between i and j, and a_{ij} is 1 if an edge exists between i and j, and 0 otherwise. This weighted version provides a more comprehensive measure of clustering in networks where edge weights are significant.

3.2.4 *Weight*

In network analysis, the weight w_{ij} of an edge between nodes i and j represents the intensity or capacity of the connection. The incorporation of weights allows for a more detailed and realistic representation of complex systems, where not all connections are equal. In this study, we operate under the assumption that all synaptic connections are equally weighted, that is to say

$$W_{ijl} = 1, \tag{5}$$

where l represents the l-th edge of node i and j. So the total weight between nodes i and j is

$$W_{ij} = Num(i,j), \tag{6}$$

where $Num(i,j)$ represents the number of synapses between neurons i and j.

3.2.5 *Strength*

In weighted networks, the concept of degree is extended to strength. The strength S_i of a node i is defined as the sum of the weights of all edges connected to it:

$$S_i = \sum_{j \in N_i} W_{ij}, \tag{7}$$

where N_i is the set of neighbors of node i and W_{ij} is the weight of the edge between i and j. This measure provides a more nuanced view of a node's importance in weighted networks, taking into account not just the number of connections, but also their intensities.

3.3 Spatial clustering method

Spatial clustering refers to the tendency of similar elements to be located near each other in physical or abstract space. In analysis, it can provide insights into the underlying structure and organization of point patterns.

Distance of points. In this study, the distance between two points refers to their Euclidean distance, unless otherwise specified. The equation of Euclidean distance is expressed as follows:

$$d(p,q) = \sqrt{\sum_{i=1}^{n}(q_i - p_i)^2}, \tag{8}$$

where $d(p,q)$ is the Euclidean distance between points p and q. n is the number of dimensions. p_i and q_i are the coordinates of p and q in the i-th dimension, respectively.

Nearest neighbor distance. The nearest neighbor distance is a fundamental concept in spatial analysis. For a point i, the nearest neighbor distance d_i is defined as the distance to its closest neighbor:

$$d_i = \min_{j \neq i}\{d_{ij}\}, \tag{9}$$

where d_{ij} is the distance between points i and j. This measure is useful for understanding the local spatial structure around individual points.

R-index. The R-index is a measure used to quantify the degree of spatial clustering in a point pattern. It is defined as

$$R = \frac{\bar{d}_O}{\bar{d}_E}, \tag{10}$$

where $\bar{d}_O$ is the observed mean nearest neighbor distance and $\bar{d}_E$ is the expected mean nearest neighbor distance in a random distribution. An R-index less than 1 indicates clustering, while an R-index greater than 1 suggests dispersion. This index provides a simple yet effective way to characterize the overall spatial distribution of points in a network.

3.4 Similarity metric: EMD

The EMD, also known as the Wasserstein metric, is a measure of the distance between two probability distributions over a region. Conceptually, it can be understood as the minimum cost of transforming one distribution into the other, where the cost is the amount of probability mass that needs to be moved, multiplied by the distance it needs to be moved.

Formally, for two distributions P and Q defined over a space X with a ground distance d, the EMD is defined as

$$\mathrm{EMD}(P,Q) = \inf_{\gamma \in \Gamma(P,Q)} \int_{X \times X} d(x,y) d\gamma(x,y), \tag{11}$$

where $\Gamma(P,Q)$ is the set of all joint distributions $\gamma(x,y)$ whose marginals are P and Q.

In practical applications, when dealing with discrete distributions or empirical samples, the EMD is often computed using linear programming techniques. For two discrete distributions $P = \{(p_i, w_{p_i})\}_{i=1}^{m}$ and $Q = \{(q_j, w_{q_j})\}_{j=1}^{n}$, where p_i and q_j are the locations and w_{p_i} and w_{q_j} are the weights, the EMD can be formulated as

$$\mathrm{EMD}(P,Q) = \min_{f_{ij}} \frac{\sum_{i=1}^{m}\sum_{j=1}^{n} f_{ij} d_{ij}}{\sum_{i=1}^{m}\sum_{j=1}^{n} f_{ij}}, \tag{12}$$

which is subject to the following constraints:

$$\begin{aligned} f_{ij} &\geqslant 0, 1 \leqslant i \leqslant m, 1 \leqslant j \leqslant n, \\ \sum_{j=1}^{n} f_{ij} &\leqslant w_{p_i}, 1 \leqslant i \leqslant m, \\ \sum_{i=1}^{m} f_{ij} &\leqslant w_{q_j}, 1 \leqslant j \leqslant n, \\ \sum_{i=1}^{m}\sum_{j=1}^{n} f_{ij} &= \min(\sum_{i=1}^{m} w_{p_i}, \sum_{j=1}^{n} w_{q_j}), \end{aligned} \tag{13}$$

where f_{ij} represents the flow from p_i to q_j, and d_{ij} is the ground distance between p_i and q_j.

The interpretation of EMD values depends on the context and the ground distance used. Generally, an EMD value of 0 indicates that the two distributions are identical. Low EMD values suggest high similarity between the distributions, while high EMD values indicate significant differences. As EMD approaches infinity, it represents maximally dissimilar distributions.

3.5 Clustering algorithms

The K-means spatial clustering algorithm [37] aims to partition n observations into k clusters in space, where each observation belongs to the cluster with the nearest mean (centroid). The algorithmic procedure is delineated as follows.

(1) Initialize: select k points as initial centroids $\{\mu_1, \mu_2, ..., \mu_k\}$ in the d-dimensional space.

(2) Assign each point x_i to the nearest centroid, forming clusters S_j,

$$S_j^{(t)} = \{x_i : \|x_i - \mu_j^{(t)}\|^2 \leqslant \|x_i - \mu_l^{(t)}\|^2 \quad \forall l, 1 \leqslant l \leqslant k\}. \tag{14}$$

(3) Update centroids to the mean of assigned points

$$\mu_j^{(t+1)} = \frac{1}{|S_j^{(t)}|} \sum_{x_i \in S_j^{(t)}} x_i. \tag{15}$$

(4) Repeat steps 2 and 3 until convergence or a maximum number of iterations is reached.

(5) Minimize the within-cluster sum of squares (WCSS):

$$\text{WCSS} = \sum_{j=1}^{k} \sum_{x_i \in S_j} \|x_i - \mu_j\|^2. \tag{16}$$

(6) Evaluate clustering quality using the silhouette coefficient

$$s(i) = \frac{b(i) - a(i)}{\max\{a(i), b(i)\}}, \tag{17}$$

where $a(i)$ is the mean distance between i and points in the same cluster, and $b(i)$ is the mean distance between i and points in the nearest different cluster.

3.6 Kuramoto model

The Kuramoto model stands as a paradigmatic framework for studying synchronization phenomena in systems of coupled oscillators, originally proposed by Yoshiki Kuramoto [38]. This mathematical model has emerged as a fundamental tool for understanding collective behavior in diverse complex systems, ranging from neural networks and chemical oscillators to power grids and biological rhythms. The model describes a population of N coupled phase oscillators, where each oscillator is characterized by its natural frequency drawn from a given probability distribution and is coupled to all other oscillators through sine functions of their phase differences. The governing equation for the i-th oscillator is given by

$$\frac{d\theta_i}{dt} = \omega_i + \frac{\lambda}{N} \sum_{j=1}^{N} \sin(\theta_j - \theta_i), \tag{18}$$

where θ_i represents the phase of the i-th oscillator, ω_i is its natural frequency, λ is the coupling strength, and N is the total number of oscillators.

The order parameter R_λ in the Kuramoto model quantifies the degree of synchronization among oscillators through a complex-valued mean field. The instantaneous order parameter is calculated as

$$z(t) = R_\lambda(t)\mathrm{e}^{\mathrm{i}\psi(t)} = \frac{1}{N}\sum_{j=1}^{N}\mathrm{e}^{\mathrm{i}\theta_j(t)}, \tag{19}$$

where $z(t)$ is the complex order parameter, $R_\lambda(t)$ is its magnitude, and $\psi(t)$ is the average phase. The practical calculation decomposes this into real and imaginary parts as

$$x(t) = \frac{1}{N}\sum_{j=1}^{N}\cos(\theta_j(t)), \tag{20}$$

and

$$y(t) = \frac{1}{N}\sum_{j=1}^{N}\sin(\theta_j(t)), \tag{21}$$

from which we obtain

$$R_\lambda(t) = \sqrt{x(t)^2 + y(t)^2}, \tag{22}$$

and

$$\psi(t) = \arctan\left(\frac{y(t)}{x(t)}\right). \tag{23}$$

We use the time-averaged order parameter

$$\langle R_\lambda\rangle = \frac{1}{T}\int_{t_0}^{t_0+T} R_\lambda(t)dt \approx \frac{1}{M}\sum_{k=1}^{M} R_\lambda(t_k), \tag{24}$$

where T is the averaging time interval and M is the number of discrete time points. The magnitude of R_λ ranges from 0 (complete desynchronization) to 1 (perfect synchronization), with intermediate values indicating partial synchronization states.

To quantify functional asymmetry between the left and right hemispheres, we define the inter-hemispheric synchronization difference

$$\Delta R_{LR}(t) = |R_L(t) - R_R(t)|, \tag{25}$$

where $R_L(t)$ and $R_R(t)$ are the instantaneous order parameters computed separately for neurons in the left and right hemispheres. The time-averaged functional asymmetry is given by $\langle\Delta R_{LR}\rangle = \frac{1}{T}\int_{t_0}^{t_0+T}\Delta R_{LR}(t)dt$. A value of $\langle\Delta R_{LR}\rangle \approx 0$ indicates functional symmetry between hemispheres, while larger values reflect stronger functional lateralization. This metric is well-defined, bounded in $[0, 1]$, and directly captures the operational difference in collective neural dynamics between the two hemispheres.

4 Discussion

In this study, we conducted a comprehensive analysis of the most extensive Drosophila brain network available to date, with a particular focus on the heterogeneity of its connectome. This heterogeneity is reflected in both the large number of neurons and their intricate connectivity patterns, especially in the highly uneven distribution of synaptic weights between neuronal pairs. Region-specific analyses further reveal substantial variability in network properties across distinct functional areas, indicating that the pronounced structural differences among these regions contribute significantly to the overall complexity of the Drosophila brain.

We also examined spatial heterogeneity within the brain network by performing global and local analyses of neuronal clustering. The results show that neuronal somata are significantly clustered throughout the brain. Moreover, most brain regions exhibit lower spatial agglomeration coefficients compared to the whole-brain average, suggesting that intra-regional clustering is more pronounced than inter-regional clustering.

Previous studies have classified neurons based on morphological, functional, and neurotransmitter-related characteristics, often leading to a single neuron being assigned to multiple functional domains [4]. To further explore

this issue, we applied spatial clustering techniques for neuron classification. However, our findings suggest that spatial proximity alone is insufficient for delineating functional neuron categories. Functional regions often comprise spatially intermixed neurons, including both intrinsic neurons and those originating from anatomically distinct areas, which complicates attempts to infer function from spatial localization alone. This observation underscores a fundamental limitation of traditional spatial parcellation approaches [39], as neurons within the same anatomically defined region may not share common functional properties.

A notable finding of our study is the strong bilateral structural symmetry between the left and right hemispheres, observed in both network topology and spatial distribution. Homologous regions across hemispheres display similar neuron and synapse counts, as well as comparable topological features. Spatial clustering characteristics are also closely matched between corresponding regions. Despite this structural symmetry, numerous studies have demonstrated lateralized functional differences in the Drosophila brain, with important implications for behavior and cognition [16, 18, 40, 41]. Such functional lateralization appears to be essential for the modulation of adaptive behaviors and other complex neurobiological processes.

Taken together, our findings suggest that structural heterogeneity and bilateral symmetry represent two complementary organizational principles operating at different scales. Inter-regional heterogeneity, which is reflected in the markedly distinct topological properties across functional regions (Figures 4 and 5), supports the functional specialization of diverse neural circuits. In contrast, inter-hemispheric symmetry, quantified by the low EMD coefficients between homologous left-right regions (Figure 6), ensures balanced and coordinated information processing across hemispheres. The localized exceptions to this symmetry (e.g., visual sensory and MBIN regions) are consistent with prior reports of asymmetric structures (e.g., the asymmetrical body [16]) and suggest that specific functional lateralizations may be structurally encoded.

While we confirmed this structural symmetry, our findings further reveal the respective contributions of intrinsic dynamics and structural connectivity to hemispheric functional asymmetry. Three complementary experiments delineate this relationship. When intrinsic frequency distributions differ between hemispheres, pronounced synchronization asymmetry emerges even under a structurally symmetric connectome (Figure 10), with ΔR_{LR} reaching values on the order of 0.2 depending on coupling strength. In contrast, when intrinsic frequencies are identical and only external stimulation is applied, inter-hemispheric differences remain consistently small (on the order of 0.03; Figure 11), indicating that frequency heterogeneity is the dominant driver of functional lateralization. Critically, when the same stimulation protocol is applied to a degree-preserving edge-swap null network, which preserves all individual neuronal degrees but destroys the specific inter-hemispheric wiring patterns, the already modest asymmetry is significantly reduced in three of four conditions (Figure 12). This demonstrates that structured connectivity pathways independently modulate, but do not dominate, stimulus-induced lateralization. Taken together, these results support a hierarchical account: intrinsic frequency differences between hemispheres serve as the primary driver of functional asymmetry, while the specific bilateral wiring of the connectome plays a secondary, modulatory role in shaping the transmission of lateralized signals. Both factors are necessary for a complete account of hemispheric functional lateralization.

Taken together, our findings provide new insights into the heterogeneous structural and functional organization of the Drosophila brain. By revealing the interplay between network topology, spatial distribution, and intrinsic dynamics, this work contributes to a deeper understanding of how brain structure supports function. Future research should investigate the developmental and evolutionary mechanisms shaping these complex patterns, particularly the balance between bilateral symmetry and functional specialization.

Looking ahead, further exploration of Drosophila brain heterogeneity from a functional perspective could illuminate its causal relationship with specific cognitive and behavioral functions. Understanding how structural diversity shapes neural computation may help uncover fundamental principles of intelligence. Moreover, the principles of heterogeneity identified in this study may inform the design of biologically inspired artificial neural networks. Investigating how structural diversity influences learning, adaptation, and efficiency in artificial systems, such as large language models, could aid the development of more robust and biologically plausible intelligent architectures.

Several limitations of the Kuramoto modeling approach should be noted. First, the model neglects synaptic conduction delays, which introduce phase shifts and could reduce synchronization levels in both hemispheres. However, because the structural connectivity is bilaterally symmetric, delays would affect both hemispheres similarly and are unlikely to systematically bias ΔR_{LR}. Second, the sine coupling in the Kuramoto model represents the weak-coupling limit of a more general phase-reduced oscillator; stronger or more complex coupling nonlinearities could produce richer dynamical regimes (e.g., multistability), but the central role of frequency heterogeneity in shaping synchronization patterns is a generic feature preserved across coupling forms. Third, our simulations operate on timescales of tens of milliseconds, which is far shorter than typical synaptic plasticity windows (seconds to minutes); plasticity is therefore unlikely to affect the transient synchronization dynamics reported here, though

it may reshape the structural substrate itself over developmental timescales, which is an intriguing direction for future work. Overall, while the specific numerical values of ΔR_{LR} may depend on model details, the qualitative conclusion that inter-hemispheric frequency differences drive functional asymmetry is expected to be robust to these simplifications.

Acknowledgements This work was supported by Brain Science and Brain-like Intelligence Technology-National Science and Technology Major Project (Grant No. 2025ZD0215703), Major Program of Xiangjiang Laboratory (Grant No. 24XJJCYJ01001), and National Natural Science Foundation of China (Grant Nos. 72421002, 92467302, 72088101, 72301285, 72474223, 12371482, 12522123).

References

1 Koch C, Laurent G. Complexity and the nervous system. Science, 1999, 284: 96–98
2 Perez N, Leung V C H, Dragotti P L, et al. Neural heterogeneity promotes robust learning. Nat Commun, 2021, 12: 5791
3 Segal A, Parkes L, Aquino K, et al. Regional, circuit and network heterogeneity of brain abnormalities in psychiatric disorders. Nat Neurosci, 2023, 26: 1613–1629
4 Zeng H, Sanes J R. Neuronal cell-type classification: challenges, opportunities and the path forward. Nat Rev Neurosci, 2017, 18: 530–546
5 Cembrowski M S, Menon V. Continuous variation within cell types of the nervous system. Trends Neuroscis, 2018, 41: 337–348
6 Huang Z J, Paul A. The diversity of GABAergic neurons and neural communication elements. Nat Rev Neurosci, 2019, 20: 563–572
7 Marder E, Taylor A L. Multiple models to capture the variability in biological neurons and networks. Nat Neurosci, 2011, 14: 133–138
8 Gjorgjieva J, Drion G, Marder E. Computational implications of biophysical diversity and multiple timescales in neurons and synapses for circuit performance. Curr Opin Neurobiol, 2016, 37: 44–52
9 Amit D J, Brunel N. Model of global spontaneous activity and local structured activity during delay periods in the cerebral cortex. Cerebral Cortex, 1997, 7: 237–252
10 Marder E, Goaillard J M. Variability, compensation and homeostasis in neuron and network function. Nat Rev Neurosci, 2006, 7: 563–574
11 Prinz A A, Bucher D, Marder E. Similar network activity from disparate circuit parameters. Nat Neurosci, 2004, 7: 1345–1352
12 Bean B P. The action potential in mammalian central neurons. Nat Rev Neurosci, 2007, 8: 451–465
13 Nusser Z. Variability in the subcellular distribution of ion channels increases neuronal diversity. Trends Neuroscis, 2009, 32: 267–274
14 Corballis M C. The evolution of lateralized brain circuits. Front Psychol, 2017, 8: 1021
15 Schmitz J, Güntürkün O, Ocklenburg S. Building an asymmetrical brain: the molecular perspective. Front Psychol, 2019, 10: 982
16 Pascual A, Huang K L, Neveu J, et al. Brain asymmetry and long-term memory. Nature, 2004, 427: 605–606
17 Turner-Evans D B, Jayaraman V. The insect central complex. Curr Biol, 2016, 26: R453–R457
18 Linneweber G A, Andriatsilavo M, Dutta S B, et al. A neurodevelopmental origin of behavioral individuality in the Drosophila visual system. Science, 2020, 367: 1112–1119
19 Konieczny L, Roterman-Konieczna I, Spólnik P. The structure and function of living organisms. In: Proceedings of Systems Biology: Functional Strategies of Living Organisms, 2023. 1–52
20 Kohn K P, Underwood S M, Cooper M M, et al. Connecting structure-property and structure-function relationships across the disciplines of chemistry and biology: exploring student perceptions. LSE, 2018, 17: ar33
21 Zhang X, Yang W, Feng J, et al. GSpect: spectral filtering for cross-scale graph classification. IEEE Trans Netw Sci Eng, 2025, 12: 547–558
22 Demirtaş M, Burt J B, Helmer M, et al. Hierarchical heterogeneity across human cortex shapes large-scale neural dynamics. Neuron, 2019, 101: 1181–1194.e13
23 Cook S J, Jarrell T A, Brittin C A, et al. Whole-animal connectomes of both Caenorhabditis elegans sexes. Nature, 2019, 571: 63–71
24 Dorkenwald S, Matsliah A, Sterling A R, et al. Neuronal wiring diagram of an adult brain. Nature, 2024, 634: 124–138
25 Lin A, Yang R, Dorkenwald S, et al. Network statistics of the whole-brain connectome of Drosophila. Nature, 2024, 634: 153–165
26 Ma X, Chen X, Zhang Y, et al. Beyond feedforward: unveiling a recurrent core and super-hubs in the Drosophila connectome. In: Proceedings of the 2026 IEEE International Conference on Pattern Recognition, Machine Vision and Artificial Intelligence (PRMVAI), 2026. 1–5
27 Chen X, Ma X, Zhang Y, et al. Topology, time, and spikes: a systematic investigation of structural and temporal interactions in neural architectures. In: Proceedings of the 2026 IEEE International Conference on Pattern Recognition, Machine Vision and Artificial Intelligence (PRMVAI), 2026. 1–5
28 Clauset A, Shalizi C R, Newman M E J. Power-law distributions in empirical data. SIAM Rev, 2009, 51: 661–703
29 Zhang X, Yang P, Feng J, et al. Network structure governs Drosophila brain functionality. Fund Res, 2026, 6: 1859–1868
30 Ivry R, Robertson L C. The Two Sides of Perception. Cambridge: MIT Press, 1997
31 Lloyd S. Least squares quantization in PCM. IEEE Trans Inform Theor, 1982, 28: 129–137
32 Shi J B, Malik J. Normalized cuts and image segmentation. IEEE Trans Pattern Anal Machine Intell, 2000, 22: 888–905
33 Murtagh F, Contreras P. Algorithms for hierarchical clustering: an overview. WIREs Data Min Knowl, 2012, 2: 86–97
34 Kong X Z, Postema M C, Guadalupe T, et al. Mapping brain asymmetry in health and disease through the ENIGMA consortium. Hum Brain Mapping, 2022, 43: 167–181
35 Wang J, Ma S, Yu P, et al. Evolution of human brain left-right asymmetry: old genes with new functions. Mol Biol Evol, 2023, 40: msad181
36 Schlegel P, Yin Y, Bates A S, et al. A consensus cell type atlas from multiple connectomes reveals principles of circuit stereotypy and variation. bioRxiv, 2023, doi: 10.1101/2023.06.27.546055
37 MacQueen J. Some methods for classification and analysis of multivariate observations. In: Proceedings of the 5th Berkeley Symposium on Mathematical Statistics and Probability, 1967. 281–297
38 Kuramoto Y. Self-entrainment of a population of coupled non-linear oscillators. In: Proceedings of International Symposium on Mathematical Problems in Theoretical Physics, 1975. 420–422
39 Eickhoff S B, Yeo B T T, Genon S. Imaging-based parcellations of the human brain. Nat Rev Neurosci, 2018, 19: 672–686
40 Abubaker M B, Hsu F Y, Feng K L, et al. Asymmetric neurons are necessary for olfactory learning in the Drosophila brain. Curr Biol, 2024, 34: 946–957
41 Lapraz F, Boutres C, Fixary-Schuster C, et al. Asymmetric activity of NetrinB controls laterality of the Drosophila brain. Nat Commun, 2023, 14: 1052